Performance of Hybrid Satellite-UAV NOMA Systems

Christina Gamal [1], Kang An [2], Xingwang Li [3], Varun G. Menon [4], Ragesh G. K. [5],
Mostafa M. Fouda [6], Basem M. ElHalawany [1,*]
[1]Faculty of Engineering at Shoubra, Benha University, Egypt
[2]Sixty-third Research Institute, National University of Defense Technology, Nanjing, China
[3]Physics and Electronic Information Engineering, Henan Polytechnic University, China
[4]SCMS School of Engineering and Technology, Ernakulam 683576, India
[5]Indian Institute of Information Technology Kottayam, India
[6]Department of Electrical and Computer Engineering, Idaho State University, Pocatello, ID, USA
*Corresponding Author, Email: basem.mamdoh@feng.bu.edu.eg

***Abstract*—This paper investigates the performance of non-orthogonal multiple access (NOMA) based hybrid satellite-unmanned aerial vehicle (UAV) systems, where a low Earth orbit (LEO) satellite communicates with the ground users via a decode and forward (DF) UAV relay. We investigate a two NOMA users system, where a far user (FU) and a near user (NU) are served by the UAV which is located at a certain height above the origin of the coverage circle. The channel between satellite and UAV is assumed to follow a Shadowed-Rician fading and the channels between UAV and users are assumed to follow a Nakagami-m fading. New closed-form expressions of the outage probabilities for the two users and the system are derived. Different from other work in literature, we take into consideration different parameters affecting the total link budget. Additionally, we propose an algorithm for minimizing the system outage probability. The mathematical analysis is verified by extensive representative Monte-Carlo (MC) simulations. Finally, simulations are provided to demonstrate the impact of important parameters on the considered system as well as the superiority of the NOMA scheme the over reference scheme.**

***Index Terms*—Outage Probability, Unmanned Aerial Vehicle, Satellite, Non-Orthogonal Multiple Access.**

I. Introduction

Recently, satellite communication (SatCom) has withdrawn an increasing research interest due to the several advantages offering over conventional terrestrial communication such as wide coverage area, covering harsh and isolated geographical regions where conventional wired or wireless communication can't reach including maritime, deserts, and jungles. Moreover, SatCom serves well in disaster areas where the terrestrial networks are compromised. Additionally, SatCom can provide a wide range of flexible applications in the field of navigation, TV and Radio broadcasting services, Weather prediction and climate monitoring, Internet access, and satellite telephony [1]. On the other hand, SatCom networks face several challenges including operation cost [2], propagation delay [3], and signal degradation due to rain and atmospheric disturbances. Additionally, antenna-pointing errors angle caused by satellite perturbation or by the other side's mobility may lead to communication outage [4]. Furthermore, the line-of-sight (LOS) link may be blocked by heavy shadowing or obstacles that retard communication between the satellite and terrestrial users [5]. To combat such issues, hybrid satellite-terrestrial networks (HSTNs) based on relaying have been proposed in many literature [2], [5]–[7] to increase efficiency, and enhance the performance of the user whose direct link is unavailable or deteriorated. Satellites can be stationed in a variety of orbits including Low Earth orbit (LEO), medium Earth orbit (MEO), highly elliptical orbit (HEO), and geosynchronous orbit (GEO) [8]. Recently, LEO satellites constellation networks have withdrawn a great interest due to their small propagation delay, high data rate, and lower transmit power [9]. Consequently, we consider a LEO satellite setup in this work.

On the other hand, unmanned aerial vehicles (UAVs) have been used as a wireless flying base station, mobile relay, or backhaul to improve the coverage, flexibility, and reliability of the network [1] in order to provide a variety of applications including reconnaissance, surveillance, disaster management, traffic control, healthcare, emergency search, military, agriculture, and communication relay [10], [11]. Thus, the combination of a UAV and a satellite has the potential to provide a technological breakthrough for communication networks due to the UAV's flexible mobility [12]–[14]. However, UAVs communication have their own challenges including limited bandwidth and limited battery [9], which mandates the exploitation of spectrum and energy efficient techniques in both transmission and mobility.

Non-orthogonal multiple access(NOMA) is one of the most promising and spectrum efficient techniques with a significant attention. NOMA improves the spectrum efficiency by serving more than one user at the same time with the same frequency resource [15], [16]. The power-domain NOMA (PD-NOMA) is the most widely used type NOMA at which a superposition of users' signals is transmitted using different power levels. However, this type of non-orthogonality causes interference at the receiver. To cope with this, successive interference cancellation (SIC) is used at the receiver to successively decode users' information one by one from the superimposing signal in the order of the received signal strength [17]. Improved spectrum efficiency, high connectivity, multiplexes many users, flexible power control method between strong and weak users, and low latency are all benefits of the NOMA scheme [18]. In contrast, the orthogonal multiple access (OMA) scheme is not the best choice to achieve the requirements for SatCom as OMA provides limit number of served users and reduced resource efficiency [4]. NOMA has been investigated for several network architectures and applications and proved to be an efficient technology [19]–[22].

To satisfy the higher throughput, low latency, higher reliability, and massive connectivity requirements of beyond fifth-generation (5G) and six-generation (6G) communications, network designers have to adopt a heterogeneous architecture that makes the best use of the advantages of different technologies [23]. This motivates researchers to investigate the performance of heterogeneous architectures of HSTN NOMA-based systems. The authors in [5] have considered the fairness issue in a NOMA-based HSTN system, where the terrestrial network acts as a cooperative relay. In [24], the NOMA-based integrated satellite-terrestrial relay networks (ISTNs) with multiple terrestrial relays was proposed, where a satellite communicates with two terrestrial users with the help of a selected relay out of multiple terrestrial relays under imperfect SIC. The performance of energy-harvesting terrestrial relay-based HSTNs network is investigated, where both amplify-and-forward (AF) [25] and decode-and-forward (DF) relay is powered from the satellite signals under NOMA transmission [2]. In [26], the authors investigated the outage probability of HSTN NOMA-based system, at which one user receives its signal directly from the satellite, while the other user relies on a multiple antenna DF relay. Further, the secrecy outage probability (SOP) of the HSTRN was investigated in [27] using physical layer security (PLS) technique in the presence of multiple eavesdroppers.

Moreover, the exploitation of aerial UAV relays is a promising direction to improve the performance of HSTRN systems. In [1], the PLS of a HSTN system with multiple mobile UAV DF relays was investigated. In [6], the authors have proposed a hybrid satellite-UAV architecture operated by a 5G non-orthogonal terrestrial network. The authors have investigated the outage probability and the asymptotic behavior where a satellite communicates with ground users with the help of a NOMA-based DF UAV relay. However, those investigations don't take into consideration the path-losses associated with satellite communication besides the antenna pointing errors [4]. This motivates researchers to investigate the performance of a practical heterogeneous HSTN NOMA system, where a UAV is used as a flying relay node. We investigate the system performance under free-space path loss and antenna pointing error, while the satellite-to-UAV and UAV-to-Terrestrial users channels undergo Shadowed-Rician and Nakagami-m fading channels, respectively. Mainly, the contributions of this work can be summarized as follows:

- We investigate the performance of a downlink NOMA-based HSTRN system that consists of a LEO satellite, DF UAV relay, and two NOMA terrestrial users. We take into consideration both small and large scale fading of satellite to UAV link under the effects of satellite beam gain, satellite antenna gain, receive antenna gain, antenna pointing error, free space loss, and noise power.
- We derive closed-form expressions for the outage probabilities (OPs) of the two users and the system OP.
- We propose an optimization algorithm that tweaks the power allocation factor to minimize the system OP.
- Validate the analytical derivations by extensive Monte-Carlo simulations, and then we study the impact of system parameters on the OPs. Finally, we carried out a comparison with a benchmark system.

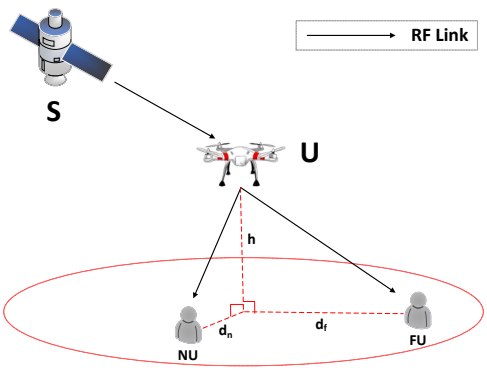

Figure 1. The system model.

II. System Model and Channel Statistics

A. System Model

We consider a downlink Satellite scenario, at which a LEO Satellite (S) communicates with terrestrial NOMA users with the aid of a DF UAV (U) relay node deployed at a constant height h from the ground, as shown in figure 1. We consider two users NOMA group, namely the far user (FU) and the near user (NU). We assume a half-duplex communication mode for all nodes, which are equipped with a single antenna. We further suppose that due to the obstruction or severe large-scale fading, direct links between the satellite and the users are unavailable, which encourages relying on the UAV as a relaying node.

Following DF relaying mechanism, S transmits a superposing signal to the two NOMA users via the UAV relay. It is assumed that the NU and FU are located inside a circle while UAV is located above the origin of the circle. We assume perfect channel state information (CSI) of all links, where the S-U link, h_s, undergoes Shadowed Rician fading distribution, whereas the links between U and ground users are subject to the Nakagami-m fading distribution. We take into consideration the free-space path loss, the receiver antenna gain, the satellite antenna gain, antenna pointing error, shadowing, and channel fading in the S-U link. Therefore, the entire link budget of the S-U link, without the small-scale fading, can be given as [28]

$$LB_s = \frac{G_s(\phi_s)\, G_u}{L_s\, L_p}, \tag{1}$$

where G_u is the UAV antenna gain, and $G_s(\phi_s)$ is the beam gain and can be formulated as $G_s(\phi_s) = G_s(\frac{J_1(u_s)}{2u_s} + 36\frac{J_3(u_s)}{u_s^3})^2$ [4] with G_s denotes the satellite antenna gain, $J(.)$ denotes the Bessel function, and $u_s = 2.07123\ \frac{d}{R}$ as R is the radius of the coverage area, d is the distance between the beam center and the UAV. L_s is the free-space loss, $L_s = \frac{4\,\pi\, f_s\, H}{c}$, where the downlink carrier frequency at satellite is f_s, the height of the satellite is H and the light velocity is c, and L_p is the pointing error loss and can be given in dB as $L_p = 2.7211 \times 10^{-20}\ f_s^2\ D_s^2\ \theta_e^2$ [29] with D_s being

the diameter of antenna aperture, and θ_e is the pointing error angle. Assuming a NOMA-based DF relaying, the end-to-end communication process from the satellite to the ground users happens in two-time slots. In the first time slot, S broadcasts a superimposing signal x_s to U, whereas $x_s = \sqrt{a_1 P_s}x_1 + \sqrt{a_2 P_s}x_2$, given that x_1 and x_2 are the signals for FU and NU, respectively. Thus, the received signal at U can be expressed as $y_{s_u} = h_s\sqrt{LB_s}x_s + n_s$, where P_s is the transmit power at S, a_1 and a_2 denote the power allocation factors for FU and NU, respectively, where $a_1 > a_2$ and $a_1 + a_2 = 1$. $n_s \sim \mathcal{CN}(0, \sigma_s^2)$ represents the additive white Gaussian noise (AWGN) with zero mean and variance $\sigma_s^2 = K\ T\ B$, where $K = 1.38 * 10^{-23}\ J/K$ is a Boltzmann's constant, B is the noise bandwidth, and T is the noise temperature. Based on the DF relaying strategy, the UAV first decodes the received signal then forwards it to the two users. So, the UAV relay decodes the signal with the high effective channel gain first then SIC is applied to decode the other signal. Thus, the received signal to interference and noise ratio (SINR) at U for signal x_1 and x_2 can be written as

$$\gamma_{x_1}^U = \frac{\gamma_s\, LB_s\, a_1|h_s|^2}{\gamma_s\, LB_s\, a_2|h_s|^2 + 1}, \tag{2a}$$

$$\gamma_{x_2}^U = \gamma_s\, LB_s\, a_2|h_s|^2, \tag{2b}$$

where $\gamma_s = \frac{P_s}{\sigma_s^2}$ denotes the transmit SNR at S, and $|h_s|^2$ is the channel power gain of satellite link that follows a shadowed Rician fading model. In the second time slot, the UAV forwards a combined version, x_u, of both decoded symbols to the paired users. Thus, the received signal at FU and NU can be expressed as $y_f = h_f\ \sqrt{P_f}\ x_u + n_f,\ \ y_n = h_n\ \sqrt{P_n}\ x_u + n_n$ respectively, where $x_u = \sqrt{b_1 P_u}x_1 + \sqrt{b_2 P_u}x_2$, P_u is the transmit power at U, h_f and h_n are the channel gain coefficients of FU and NU, respectively. P_n and P_f are the path losses at NU and FU respectively and can be written as $\frac{\delta_l}{(\sqrt{d_i^2+h^2})^\alpha}$, d_i represents the propagation distance between the UAV and ground user, δ_l denotes the frequency dependent channel power at the reference distance of 1m, and α is the path-loss exponent [30]. $n_f \sim \mathcal{CN}(0, \sigma_f^2)$ and $n_n \sim \mathcal{CN}(0, \sigma_n^2)$ represent the additive white Gaussian noise (AWGN) at FU and NU respectively. b_1 and b_2 denote the power allocation factors for FU and NU respectively, where $b_1 > b_2$ and $b_1 + b_2 = 1$. Thus, the received SINR at FU is:

$$\gamma_{x_1}^f = \frac{\gamma_f\, P_f\, b_1|h_f|^2}{\gamma_f\, P_f\, b_2|h_f|^2+1}, \tag{3}$$

where $\gamma_f = P_u/{\sigma_f}^2$ denotes the transmit SNR at U to FU. The near user decode FU's signal first then SIC is applied to get NU's signal. Thus, the received SINR at NU for x_1 and x_2 can be expressed as

$$\gamma_{x_1}^n = \frac{\gamma_n\, P_n\, b_1|h_n|^2}{\gamma_n\, P_n\, b_2|h_n|^2 + 1}, \tag{4a}$$

$$\gamma_{x_2}^n = \gamma_n\, P_n\, b_2|h_n|^2, \tag{4b}$$

where γ_n denotes the transmit SNR at U to NU, and $\gamma_n = \gamma_f = \gamma_u$.

B. Channel Statistics

The satellite to UAV link undergoes a shadowed-Rician fading, where the probability density function (PDF) of $|h_s|^2$ is [27]:

$$f_{|h_s|^2}(x) = \alpha_s \exp\left(-\beta_s x\right)\ {}_1F_1\left(m_s; 1; \delta_s x\right), \tag{5}$$

where $\alpha_s = \frac{1}{2\,b_s}\left(\frac{2\,b_s\,m_s}{2\,b_s\,m_s+\Omega_s}\right)^{m_s}$, $\beta_s = \frac{1}{2\,b_s}$, and $\delta_s = \frac{\Omega_s}{2\,b_s\,(2\,b_s\,m_s+\Omega_s)}$. ${}_1F_1(.;.;.)$ is the confluent hypergeometric function of the first kind [31, Eq. (9.14.1)], m_s denotes the fading severity parameter, Ω_s represents the average power of line-of-sight (LOS) and $2\,b_s$ represents the multipath components. With the aid of equations [32, (07.20.03.0009.01)] and [33, (07.02.03.0014.01)], ${}_1F_1$ function can be expressed as

$${}_1F_1\left(m_s; 1; \delta_s x\right) = e^{\delta_s x} \sum_{k=0}^{m_s-1} \frac{(-1)^k(1-m_s)_k(\delta_s x)^k}{(k!)^2}, \tag{6}$$

where $(.)_n$ is the pochhammer symbol [31, p. xliii]. Let $\zeta(k) = \frac{(-1)^k(1-m_s)_k(\delta_s)^k}{(k!)^2}$. With the help of equation [31, (3.351.2)], the cumulative distribution function (CDF) of the $|h_s|^2$ is expressed as

$$\begin{aligned} F_{|h_s|^2}(x) = 1 - \alpha_s\, e^{-(\beta_s-\delta_s)x} \sum_{k=0}^{m_s-1} \zeta(k) \\ \times \sum_{l=0}^{k} \frac{k!}{l!}\, x^l\ (\beta_s - \delta_s)^{-(k-l+1)}. \end{aligned} \tag{7}$$

The links between the UAV relay and the FU and NU are assumed to follow the Nakagami-m fading whose PDF $|h_i|^2$, $i \in \{f, n\}$ can be expressed as [34]

$$f_{|h_i|^2}(x) = \left(\frac{m_i}{\Omega_i}\right)^{m_i}\ \frac{x^{m_i-1}}{\Gamma(m_i)}\ e^{-\frac{m_i}{\Omega_i}x}, \tag{8}$$

and the CDF of $|h_i|^2$ is expressed as

$$F_{|h_i|^2} = 1 - e^{-\frac{m_i}{\Omega_i}x} \sum_{n=0}^{m_i-1} \left(\frac{m_i}{\Omega_i}x\right)^n\ \frac{1}{n!}, \tag{9}$$

where m_i is the severity parameter for user i.

III. Outage probability Analysis

In this section, we investigate the reliability of the proposed system, where the reliability is characterized in terms of the users and system outage probabilities (OPs). The OP is the probability that a specific SINR falls below a certain threshold value. In the following, we derive the OPs of both users and the system OP as follows:

1) OP of NU (OP_n): The OP event for NU occurs when neither the UAV nor the NU correctly decodes x_1 and x_2, which can be mathematically expressed as [6]

$$\begin{aligned} OP_n &= \Pr(\min(\tfrac{\gamma_{x_1}^U}{\gamma_{th_f}}, \tfrac{\gamma_{x_2}^U}{\gamma_{th_n}}) < 1) + \\ &\quad \Pr(\min(\tfrac{\gamma_{x_1}^U}{\gamma_{th_f}}, \tfrac{\gamma_{x_2}^U}{\gamma_{th_n}}) \geq 1,\ \min(\tfrac{\gamma_{x_1}^n}{\gamma_{th_f}}, \tfrac{\gamma_{x_2}^n}{\gamma_{th_n}}) < 1) \\ &= 1\ - \Pr(\gamma_{x_1}^U \geq \gamma_{th_f},\ \gamma_{x_2}^U \geq \gamma_{th_n}) \\ &\quad \times \Pr(\gamma_{x_1}^n \geq \gamma_{th_f},\ \gamma_{x_2}^n \geq \gamma_{th_n}), \end{aligned} \tag{10}$$

where $\gamma_{th_f} = 2^{2R_f} - 1$ and $\gamma_{th_n} = 2^{2R_n} - 1$ are the target SINR threshold at FU and NU, respectively. R_f and R_n are

the target data rates for FU and NU respectively. From (2) and (4), the OP_n in (10) can be written as,

$$\begin{aligned} OP_n &= 1 - \Pr(|h_s|^2 \geq \max(\tfrac{\gamma_{th_f}\,\omega_1}{a_1 - a_2\,\gamma_{th_f}}, \tfrac{\gamma_{th_n}\,\omega_1}{a_2})) \\ &\times \Pr(|h_n|^2 \geq \max(\tfrac{\gamma_{th_f}\,\omega_2}{b_1 - b_2\,\gamma_{th_f}}, \tfrac{\gamma_{th_n}\,\omega_2}{b_2})) \\ &= 1 - \big(1 - F_{|h_s|^2}(A\,\omega_1)\big)\ \times (1 - F_{|h_n|^2}(B\,\omega_2)), \end{aligned} \tag{11}$$

such that $a_1 - a_2\gamma_{th_f} > 0$ and $b_1 - b_2\gamma_{th_f} > 0$ and $OP_n = 1$ otherwise, where $A = \max\big(\frac{\gamma_{th_f}}{a_1 - a_2\,\gamma_{th_f}}, \frac{\gamma_{th_n}}{a_2}\big)$, $B = \max(\frac{\gamma_{th_f}}{b_1 - b_2\,\gamma_{th_f}}, \frac{\gamma_{th_n}}{b_2})$, $\omega_1 = \frac{1}{\gamma_s L B_s}$, and $\omega_2 = \frac{1}{\gamma_u P_n}$. By substituting (7), and (9) into (11), the closed-form expression for the OP_n can be expressed as,

$$\begin{aligned} OP_n = 1 - \alpha_s\, e^{-(\beta_s - \delta_s)A\omega_1} \textstyle\sum_{k=0}^{m_s-1} \zeta(k) \sum_{l=0}^{k} \frac{k!}{l!}\,(A\omega_1)^l \\ \times(\beta_s - \delta_s)^{-(k-l+1)}\, e^{-\frac{m_n}{\Omega_n}B\omega_2} \textstyle\sum_{n=0}^{m_n-1} (\frac{m_n}{\Omega_n}B\omega_2)^n\ \frac{1}{n!}. \end{aligned} \tag{12}$$

2) OP of FU (OP_f): The outage event will occur for the FU when the UAV is unable to decode x_1, x_2, or when the UAV is able to decode x_1 and x_2, but the FU is unable to decode its signal. Consequently, the OP_f can be stated as [6]

$$\begin{aligned} OP_f &= \Pr(\min(\tfrac{\gamma^U_{x_1}}{\gamma_{th_f}}, \tfrac{\gamma^U_{x_2}}{\gamma_{th_n}} < 1) + \\ &\Pr(\min(\tfrac{\gamma^U_{x_1}}{\gamma_{th_f}}, \tfrac{\gamma^U_{x_2}}{\gamma_{th_n}} \geq 1), \tfrac{\gamma^f_{x_1}}{\gamma_{th_f}} < 1) \\ &= \Pr(\min(\tfrac{\gamma^U_{x_1}}{\gamma_{th_f}}, \tfrac{\gamma^U_{x_2}}{\gamma_{th_n}}, \tfrac{\gamma^f_{x_1}}{\gamma_{th_f}}) < 1) \\ &= 1 - \Pr(\gamma^U_{x_1} \geq \gamma_{th_f}, \gamma^U_{x_2} \geq \gamma_{th_n}, \gamma^f_{x_1} \geq \gamma_{th_f}). \end{aligned} \tag{13}$$

Similar to the derivation of the OP for the NU, the closed-form expression for OP_f can be expressed as

$$\begin{aligned} OP_f = 1 - \alpha_s\, e^{-(\beta_s - \delta_s)A\omega_1} \textstyle\sum_{k=0}^{m_s-1} \zeta(k) \sum_{l=0}^{k} \frac{k!}{l!}\,(A\omega_1)^l \\ \times(\beta_s - \delta_s)^{-(k-l+1)}\, e^{-\frac{m_f}{\Omega_f}C\omega_3} \textstyle\sum_{n=0}^{m_f-1} (\frac{m_f}{\Omega_f}C\omega_3)^n\ \frac{1}{n!}, \end{aligned} \tag{14}$$

where $C = \frac{\gamma_{th_f}}{b_1 - b_2\,\gamma_{th_f}}$, and $\omega_3 = \frac{1}{\gamma_u P_f}$.

3) The System OP (OP_{sys}): can be expressed as

$$\begin{aligned} OP_{sys} = 1 - \Pr(\gamma^U_{x_1} \geq \gamma_{th_f}, \gamma^U_{x_2} \geq \gamma_{th_n}) \\ \times \Pr(\gamma^f_{x_1} \geq \gamma_{th_f}, \gamma^n_{x_1} \geq \gamma_{th_f}, \gamma^n_{x_2} \geq \gamma_{th_n}), \end{aligned} \tag{15}$$

By substituting (2), (3), and (4) into (15), and using (7) and (9), the closed form expression of the OP_{sys} is given as

$$\begin{aligned} OP_{sys} = 1 - \alpha_s\, e^{-(\beta_s - \delta_s)A\omega_1} \textstyle\sum_{k=0}^{m_s-1} \zeta(k) \sum_{l=0}^{k} \frac{k!}{l!}\, A\omega_1{}^l \\ \times(\beta_s - \delta_s)^{-(k-l+1)}\, e^{-\frac{m_n}{\Omega_n}B\omega_2} \textstyle\sum_{n=0}^{m_n-1} (\frac{m_n}{\Omega_n}B\omega_2)^n\ \frac{1}{n!} \\ \times e^{-\frac{m_f}{\Omega_f}C\omega_3} \textstyle\sum_{u=0}^{m_f-1} (\frac{m_f}{\Omega_f}C\omega_3)^u\ \frac{1}{u!}. \end{aligned} \tag{16}$$

IV. Optimization Algorithm for Power Allocation

In this section, we propose the following optimization algorithm for adjusting the power allocation factor to obtain the minimum system OP. We assume that $a_1 = b_1 = f_1$ and $\gamma_{th_n} = \gamma_{th_f} = \gamma_{th}$, which can be written as:

$$\min_{f_1} \quad OP_{sys} \tag{17a}$$

$$s.t. \quad \frac{\gamma_{th}}{1 + \gamma_{th}} < f_1 < 1 \tag{17b}$$

The problem in (17) is convex and can be solved using any commercial solver such as Matlab and Mathematica. Figure 2 depicts the variations of the three OPs versus f_1 to show the convexity graphically. By setting the parameters in Table I and set γ_{th}= 1, the optimal system OP is achieved at f_1^* = 0.7302. In Section V, this optimization algorithm is used in all figures unless otherwise mentioned. Additionally, the convexity of the problem in (17) can be proved mathematically by differentiating OP_{sys} in (16). Based on the definition of A = B = max(η_1,η_2) for $b_1 = a_1$, where $\eta_1 = \frac{\gamma_{th}}{f_1 - f_2\,\gamma_{th}}$, $\eta_2 = \frac{\gamma_{th}}{f_2}$, $f_2 = 1 - f_1$, we divide (16) into two intervals according to the value of f_1. The first interval is $\frac{\gamma_{th}}{1+\gamma_{th}} < f_1 < \frac{1+\gamma_{th}}{2+\gamma_{th}}$, where $\eta_1 > \eta_2$ and A = B = η_1. By substituting in (16) and with some simple mathematical manipulation, the partial derivative $\frac{\partial OP_{sys}}{\partial f_1}$ can be proved to be a negative value, which means a decreasing function of f_1. Moreover, within the second interval, $\frac{(1+\gamma_{th})}{(2+\gamma_{th})} < f_1 < 1$, we can substitute A = B = η_2, where the derivative can be proved to be positive. This proves that the system OP shows an inflection point at $\frac{(1+\gamma_{th})}{(2+\gamma_{th})}$. Additionally, the second derivative $\frac{\partial^2 OP_{sys}}{\partial f_1^2}$ can be easily proved to be a positive value showing the convexity of the function with respect to f_1.

Table I
System Parameters.

Parameter	Value
Height of LEO satellite (iridium)	780 Km
Downlink carrier frequency at satellite	1.55 GHz
UAV antenna gain	1 dB
Satellite antenna gain	30 dB
Diameter of satellite antenna aperture	2 m
Pointing error angle of satellite	1°
Carrier frequency at UAV	2 GHz
The height of UAV	100 m
Horizontal distance from the UAV to the near user	50 m
Horizontal distance from the UAV to the far user	100 m
Coverage radius of spot beam from satellite (R)	200 Km
The distance from the beam center to the UAV	0.3R m
Noise bandwidth	12 MHz
Temperature noise	290 K

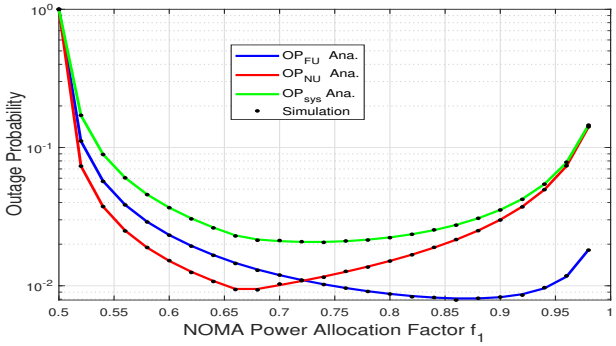

Figure 2. Outage probability versus power allocation f_1.

V. Results and Discussions

In this section, we validate the analytical results using representative numerical simulations. We evaluate the outage probability of both the satellite-UAV-terrestrial users and the system in addition to investigating the impact of key parameters on the performance. Monte-Carlo simulation is implemented to verify the accuracy by averaging over 10^6 channels realizations. For numerical analysis, we set the power allocation factor to the output of the optimal power allocation algorithm in (17). The target rates of near user and far user are assumed to be equal, where $R_n = R_f = 0.5$ unless mentioned otherwise, while $\alpha = 2$ is the path-loss factor and ${\sigma_f}^2 = {\sigma_n}^2$ = -70 dB. The link among satellite and UAV undergoes frequent heavy shadowing (FHS), the channel coefficients of terrestrial link are $m_n = m_f = 1$, $\Omega_n = \Omega_f = 1$. The settings are summarized in Table I [35].

Figure 3 plots the variations of OPs of FU, NU, and the overall system versus the transmit power compared with OMA scheme, where the transmit power $(P_t) = P_s = P_u$. The results show that the curves of theoretical analysis coincide with the Monte Carlo simulation curves, which validates our analysis. The results show that the OP improves with the increase of the transmitted power for both users under both NOMA and OMA schemes. The OPs of the far and near users are notably reduced by adopting the NOMA scheme compared with OMA scheme.

Figure 4 plots the variations of the OPs of both users as a function of the UAV height for an P_t = 35 dB for both Satellite and UAV. The results show that OP decreases when the UAV is close to the ground. It is noteworthy that FU is more sensitive to the height of the UAV than NU.

Figure 5 plots the OPs for both users versus the satellite antenna pointing error angle θ_e at fixed P_t = 35 dB. It is shown that the pointing error angle has a significant effect on the outage performance of both users, where the OP deteriorates as the pointing error angle increases. It is noteworthy that the results show a complete outage, i.e., OP = 1, for a pointing error angle around θ_e = 12°. The results in Figure 6 support those in Figure 5, it can be clearly seen that θ_e significantly influences the OP at a low value (i.e. θ_e = 7° or 9°), the OPs for both far and near user significantly decrease for the entire range of the transmitted power.

Figure 7 depicts the impact of shadowing parameters for the shadowed Rician link of the S-U channel on the OP performance. We compare the OP performance for two different shadowing scenarios, i.e., FHS, and infrequent light shadowing (ILS) whose channel parameters are given in Table II [24]. The results show that the OPs of both users under FHS scenario are slightly higher than the OPs of ILS due to the impact of communication conditions between satellite and UAV.

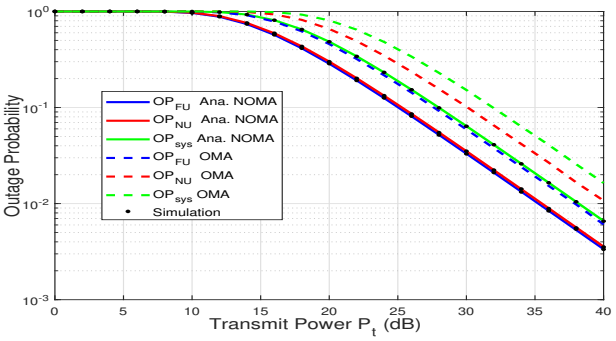

Figure 3. OP versus P_t at $R_n = R_f = 0.5$.

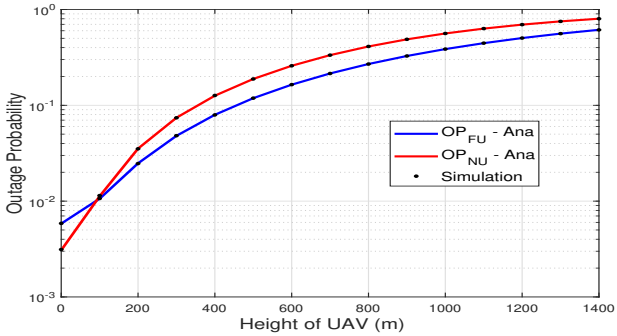

Figure 4. OP versus the height of UAV.

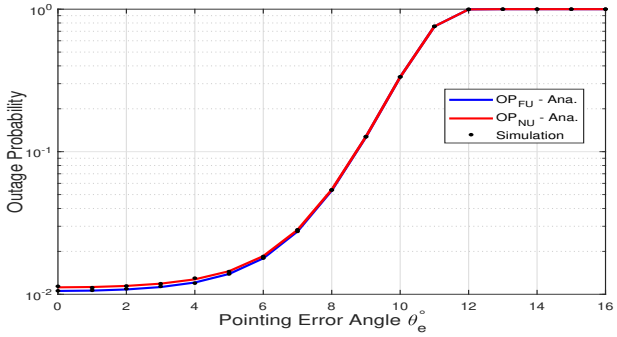

Figure 5. OP versus Pointing Error Angle.

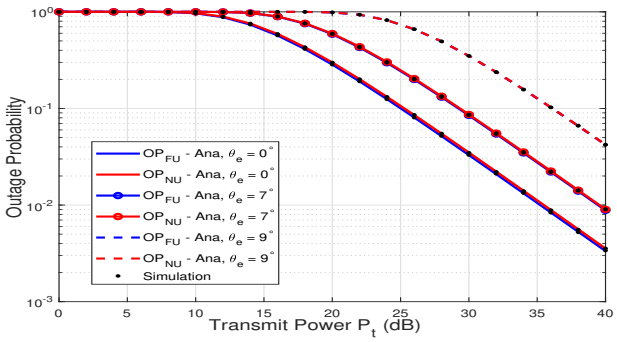

Figure 6. OP versus P_t for different pointing error angle.

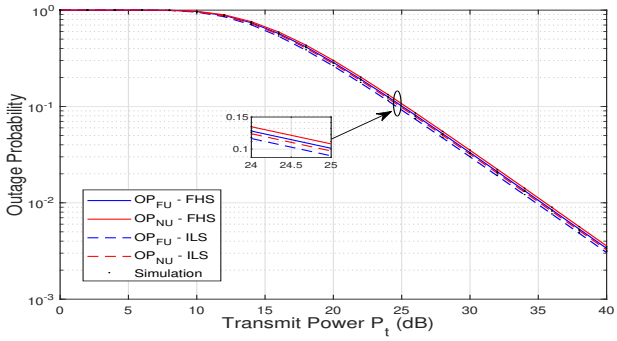

Figure 7. OP versus P_t for various shadowing parameters.

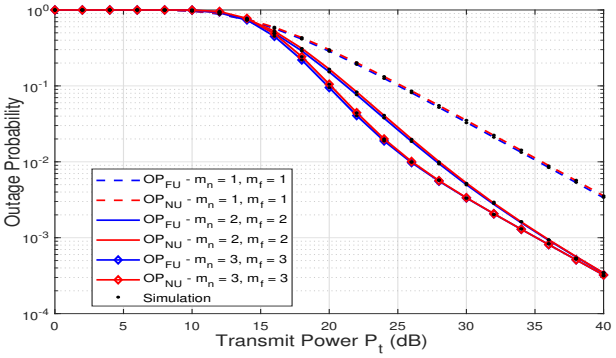

Figure 8. OP versus P_t for different Nakagami-m severity factor.

Table II
SHADOWING PARAMETERS.

Shadowing	m_s	b_s	Ω_s
Frequent heavy shadowing	1	0.063	0.0007
Infrequent light shadowing	10	0.158	1.29

Figure 8 indicates the impact of different severity conditions for the terrestrial link on the OP. The severity parameters of the terrestrial link have a significant impact on the OP. It can be seen that the OP degrades as the fading severity increases with decreasing m_i. This is because of the fact that the performance of the system enhances as the fading severity decreases.

VI. CONCLUSION

In this article, we studied the performance of the hybrid satellite-UAV-terrestrial downlink NOMA system where the closed-form expression for the outage probability is derived and evaluated with the presence of path loss and antenna-pointing error loss. We showed the impact of various parameters on the considered system. We also showed how the power allocation factor affects the total system OP and how to get an optimal power allocation. The numerical results showed the superiority of the NOMA over OMA system.

REFERENCES

[1] P. K. Sharma and D. I. Kim, "Secure 3D mobile UAV relaying for hybrid satellite-terrestrial networks," *IEEE Transactions on Wireless Communications*, vol. 19, no. 4, pp. 2770–2784, 2020.

[2] D.-T. Do et al., "Hybrid satellite-terrestrial relay network: Proposed model and application of power splitting multiple access," *Sensors*, vol. 20, no. 15, p. 4296, 2020.

[3] B. Di, L. Song, Y. Li, and H. V. Poor, "Ultra-dense LEO: Integration of satellite access networks into 5G and beyond," *IEEE Wireless Commun.*, vol. 26, no. 2, pp. 62–69, 2019.

[4] X. Yan, H. Xiao, K. An, G. Zheng, and S. Chatzinotas, "Ergodic capacity of NOMA-based uplink satellite networks with randomly deployed users," *IEEE Systems Journal*, vol. 14.

[5] X. Zhang et al., "Performance analysis of NOMA-based cooperative spectrum sharing in hybrid satellite-terrestrial networks," *IEEE Access*, vol. 7, pp. 172 321–172 329, 2019.

[6] X. Li et al., "A unified framework for HS-UAV NOMA networks: Performance analysis and location optimization," *IEEE Access*, vol. 8, pp. 13 329–13 340, 2020.

[7] X. Yan et al., "Hybrid satellite terrestrial relay networks with cooperative non-orthogonal multiple access," *IEEE Commun. Lett.*, vol. 22, no. 5, pp. 978–981, 2018.

[8] A. H. Hashim, F. D. Mahad, S. M. Idrus, and A. S. M. Supa'at, "Modeling and performance study of inter-satellite optical wireless communication system," in *International Conference On Photonics 2010*, 2010.

[9] M. R. H. Khan, M. O. Ziad, S. M. Chowa, M. Mehedi *et al.*, "A comparative study of intelligent reflecting surface and relay in satellite communication," Ph.D. dissertation, Brac University, 2021.

[10] X. Lei, L. Yang, J. Zhang, G. Li, and J. Chen, "LAP-based FSO-RF cooperative NOMA systems," in *Proc. IEEE VTC2020-Fall*, 2020.

[11] S. H. Alsamhi et al., "Green internet of things using UAVs in B5G networks: A review of applications and strategies," *Ad Hoc Networks*, p. 102505, 2021.

[12] M. Petkovic and M. Narandzic, "Overview of UAV based free-space optical communication systems," in *International Conference on Interactive Collaborative Robotics*. Springer, 2019, pp. 270–277.

[13] R. Ruby, B. M. ElHalawany, and K. Wu, "Impact of UAV mobility on physical layer security," in *Proc. IEEE MSN 2021*, 2021.

[14] R. Ruby, K. Wu, Q.-V. Pham, and B. M. ElHalawany, "Aiding a disaster spot via an UAV-based mobile AF relay: Joint trajectory and power optimization," in *Proc. ACM Symposium on Mobility Management and Wireless Access*, 2020, p. 105–113.

[15] M. V. Jamali, S. M. Azimi-Abarghouyi, and H. Mahdavifar, "Outage probability analysis of uplink NOMA over ultra-high-speed FSO-backhauled systems," in *Proc. IEEE GC Wkshps*, 2018.

[16] B. M. ElHalawany et al., "Performance analysis of downlink NOMA systems over κ-μ shadowed fading channels," *IEEE Trans. on Vehic. Tech.*, vol. 69, no. 1, pp. 1046–1050, 2020.

[17] F. Aveta and H. H. Refai, "Free space optical non-orthogonal multiple access experimentation," in *Free-Space Laser Communications XXXI*, vol. 10910. International Society for Optics and Photonics, 2019, p. 109101O.

[18] M. Najafi, V. Jamali, P. D. Diamantoulakis, G. K. Karagiannidis, and R. Schober, "Non-orthogonal multiple access for FSO backhauling," in *Proc. IEEE WCNC*, 2018.

[19] W. U. Khan et al., "Energy efficiency maximization for beyond 5G NOMA-enabled heterogeneous networks," *Peer-to-Peer Netw. Appl.*, vol. 14, no. 1, p. 3250–3264, 2021.

[20] W. U. Khan, F. Jameel, T. Ristaniemi, B. M. Elhalawany, and J. Liu, "Efficient power allocation for multi-cell uplink NOMA network," in *Proc. IEEE VTC2019-Spring*, 2019.

[21] W. U. Khan, M. A. Javed, T. N. Nguyen, S. Khan, and B. M. Elhalawany, "Energy-efficient resource allocation for 6G backscatter-enabled NOMA IoV networks," *IEEE Trans. Intell. Transp. Syst.*, 2021, doi: 10.1109/TITS.2021.3110942.

[22] M. Elsayed, A. Samir, A. A. A. El-Banna, X. Li, and B. M. ElHalawany, "When NOMA multiplexing meets symbiotic ambient backscatter communication: Outage analysis," *IEEE Trans. Vehic. Technology*, vol. 71, no. 1, pp. 1026–1031, 2022.

[23] P. S. Bithas et al., "A survey on machine-learning techniques for UAV-based communications," *Sensors*, vol. 19, no. 23, p. 5170, 2019.

[24] H. Shuai, K. Guo, K. An, and S. Zhu, "NOMA-based integrated satellite terrestrial networks with relay selection and imperfect SIC," *IEEE Access*, vol. 9, pp. 111 346–111 357, 2021.

[25] B. M. ElHalawany, M. Elsabrouty, O. Muta, A. Abdelrahman, and H. Furukawa, "Joint energy-efficient single relay selection and power allocation for analog network coding with three transmission phases," in *Proc. IEEE VTC Spring*, 2014.

[26] L. Han, W.-P. Zhu, and M. Lin, "Outage of noma-based hybrid satellite-terrestrial multi-antenna df relay networks," *IEEE Wireless Communications Letters*, vol. 10, no. 5, pp. 1083–1087, 2021.

[27] V. Bankey et al., "Physical layer security in hybrid satellite-terrestrial relay networks," in *Physical Layer Security*. Springer, 2021, pp. 1–28.

[28] X. Zhang et al., "NOMA-based proactive content caching in hybrid satellite-aerial-terrestrial networks," in *Proc. IEEE WCNCW*, 2021.

[29] G. Maral, M. Bousquet, and Z. Sun, *Satellite communications systems: systems, techniques and technology*. John Wiley & Sons, 2020.

[30] A. A. Khuwaja, Y. Chen, and G. Zheng, "Effect of user mobility and channel fading on the outage performance of UAV communications," *IEEE Wireless Commun. Lett.*, vol. 9, no. 3, pp. 367–370, 2019.

[31] D. Zwillinger and A. Jeffrey, *Table of integrals, series, and products*. Elsevier, 2007.

[32] Wolfram, the wolfram functions site, 2017. [Online]. Available: http://functions.wolfram.com/PDF/Hypergeometric1F1.pdf

[33] Wolfram, the wolfram functions site, 2017. [Online]. Available: http://functions.wolfram.com/PDF/LaguerreLGeneral.pdf

[34] S. M. Ibraheem et al., "Outage performance of NOMA-based DF relay sharing networks over Nakagami-m fading channels," in *Proc. ICCES*, 2018, pp. 512–517.

[35] S. Dey, D. Mohapatra, and S. Archana, "An approach to calculate the performance and link budget of LEO satellite (iridium) for communication operated at frequency range (1650–1550) mhz," *Int. J. Latest Trends Eng. Technol.*, vol. 4, no. 4, pp. 96–103, 2014.